

## Robust Estimation of Pre-Contact Object Trajectories

G. Petryk and M. Buehler

Department of Mechanical Engineering  
Centre for Intelligent Machines, McGill University  
3480 University Street, McConnell 423  
Montréal, QC H3A 2A7, CANADA  
buehler@cim.mcgill.ca

### Abstract

*Accurate and high bandwidth robot control for grasping and manipulation is greatly facilitated by continuous and high bandwidth sensing of the states of the object to be grasped. To this end we describe a new sensory system and the associated signal processing, using miniature intensity-based electro-optical proximity sensors, small enough to be directly embedded in a robot's end effector. In situations where the geometry of the object to be grasped is known, sensor fusion via an extended Kalman filter provides an estimate of the object's planar position, velocity and surface reflectance properties. Experimental results show robust estimation of the object's states as well as its surface properties despite noisy sensor data and unmodelled object dynamics.*

**Keywords:** Sensor fusion, Proximity Sensor Network, Electro-optical proximity sensing, Grasping, Manipulation

## 1 Introduction

Our earlier work on dynamic manipulation [1] via robotic juggling and catching tasks relied on the availability of continuous task level feedback in the form of a custom built planar inductive sensor. High rate task level sensing permitted the development of simple feedback algorithms which achieved relatively complex and dextrous robotic tasks. Subsequent work by Rizzi and Koditschek [17] succeeded to develop a spatial version of the juggling tasks using off-the-shelf cameras. Nevertheless, implementing grasping and manipulation tasks with robotic grippers or fingers will be greatly facilitated by close range sensing and the absence of camera occlusion. For purposes of object tracking, cameras are most versatile. How-

ever, when used in close proximity to objects in grasping tasks, cameras can encounter problems with lighting, focusing, sensing bandwidth, size, and occlusion. Lighting, focusing, and occlusion problems are most severe at the most inopportune time – when the object is close to the end-effector just prior to contact. "Local sensing" is needed.

The ideal local sensor is small enough to be integrated directly in a robot's gripper or finger, and should fit within a cylinder of 1 cm diameter and 2 cm length. In addition, the sensor should not contain any moving parts, like rotating mirrors, and the area of exposed optics should be minimal. In order to control high bandwidth micro-manipulators, or the fingers of the Sarcos Dextrous Arm [5], a sensing rate of 500 Hz - 1 kHz is desirable. Finally, given close proximity to objects, and the resulting lighting conditions, an active sensor is required.

Active electro-optical proximity sensors have the potential to satisfy all the aforementioned requirements, and they have a long history in the robotics research community [3, 6]. These devices work in the infra-red spectrum and can exploit one of three operating principles. *Triangulation*-based sensors tend to be the most accurate and have only a minor dependence on the object's reflective properties. But due to geometric sensing constraints imposed by triangulation, they are as large as miniature cameras and have limited close range [8, 18]. A new operating principle has recently been proposed by Masuda [14]. From the *phase shift* of the received signal, distance or orientation can be measured depending on the mode of operation. The sensor consists of six LEDs in a cross shaped pattern with the photo transistor in the center. Goldenberg et al. [15] show how this sensor's design parameters affect its performance and propose an optimal sensor design. Two drawbacks of this approach are the required base line

separation of the sensors of several centimeters, making it no smaller than triangulation based sensors, and the elaborate and thus costly signal processing electronics.

The third approach, used by *intensity-based* electro-optical proximity sensors, attempts to relate the intensity of the reflected light to sensor-object distance. However, the sensor signal depends not only on distance, but also on ambient light, the object’s reflective properties, and the angle between sensor beam and the object’s surface. Thus the most common use of this sensor in the literature is for object tracking and centering operations, or obstacle avoidance, where absolute distance measurements are not required. Relatively few previous papers, summarized in the table below, have proposed solutions to subsets of the problems to obtain proximity information. Espiau and Catros [4] examine different filtering approaches to estimate the linear sensor-object distance. Wampler [19] uses directly the calibrated voltage-distance relation, assuming known and constant reflectance and no angle dependence. More recently, Y. Li [10, 11, 12, 13] has estimated a flat object’s distance or orientation (with three sensors), using an Extended Kalman Filter (EKF), assuming a negligible angle dependence and known reflective properties (except in [13]). The simplifying assumptions in [12] allow a simple two parameter extended Kalman filter to be used since only the sensor-object distance and reflectance parameters need be estimated. In addition, only the perpendicular distance is estimated thus eliminating the need for concurrent estimation of object surface angle.

	<i>Estimation Scheme</i>	<i>States Estimated</i>
Espiau & Catros [4] (1980)	EKF, IEKF, composed, Gaussian, 2. order	1D position
Wampler [19] (1984)	Interpolation in Sensor Calibration Data Set	1D position, Orientation
Li [10] (1991)	EKF	1D position
Li [11] (1993)	3 indep. EKFs	1D position, Orientation
Li [12] (1994)	EKF	1D position
Li [13] (1994)	EKF	1D position, Const. Refl. Gain
Petryk & Buehler (here)	EKF	<b>2D position, 2D velocity, Varying Refl. Gain</b>

In order to provide practical local sensing for grasping and manipulation, several issues have to be addressed simultaneously: The sensors’ angle dependence must be considered. In addition, all

past research mentioned above has only considered measuring the distance to flat surfaces – instead “graspable” objects like cylinders, with a circular footprint should be considered. Given the strong dependence of the sensors’ output on surface properties, these should be estimated online. We describe an approach which accomplishes all these requirements. This is possible by assuming a known object geometry, and using this information for sensor fusion of several sensor outputs via an extended Kalman filter. The assumption of known object geometry is reasonable in most practical situations. This framework permits the simultaneous estimation of the object’s reflectance properties, allows for angle dependent sensor models, all while tracking an unknown object trajectory.

A previous paper [16] showed preliminary experimental results when the object’s motion was modelled correctly. Here, the full estimation problem is solved, where the object’s motion departs substantially from the model. In addition, we present experimental data which track the object’s changing reflectance properties. The paper is organized as follows. Sec. 2 introduces the Proximity Sensing Network (PSN) and its sensors. Sec. 3 describes the PSN sensor fusion via an extended Kalman filter, and the object model and any simplifying assumptions. The experimental results are shown and analyzed in Sec. 4.

## 2 Proximity Sensor Network

### 2.1 Sensor Hardware

The basic mode of operation of amplitude based electro-optical proximity sensors is very simple: An Light Emitting Diode (LED) emits a beam of infra-red light. Upon encountering a surface, part of this energy is reflected back to the receiver, which can be a Phototransistor or a PIN Diode. The strength of the received signal depends on the distance of the surface. The key advantages of this approach are evident. *Size*: The transmitter-receiver pair can be located side-by-side. With off-the-shelf 1.5 mm diameter units, very small sensor heads can be built. For ease of construction, we designed our sensor head for an external diameter of 7.8 mm, and a 5 mm diameter is readily achievable. Custom heads can be miniaturized much further. *Cost*: Robotics and Automation is very cost sensitive. Infrared sensor can use inexpensive electronics components, without additional optics. *Ruggedness*: Proximity sensors, by definition, are located close to (often hard) objects, and are prone to high accelerations due to impacts. With their small size, absence of delicate optics, they are shock resistant and rugged.

While there is an increasing number of commercial IR proximity sensors available, they are used

as threshold sensors, tuned for a particular type of object and a desired detection distance. Units which provide an optional analog output have typically very low bandwidth and would have to be modified for the multiplexed operation necessary in a sensor network. Therefore we developed our own sensor heads and processing electronics.

The ambient light influence on the received signal is rejected in hardware, by modulating the transmitted signals at 50 kHz and filtering the output of the photo-transistor through a band-pass filter tuned to this frequency. The sensor head consist of four miniature IR-LEDs which provides a detection range of up to 20 cm. Four sensors connect for amplification, filtering, multiplexing and gain scheduling to a small printed circuit board with a microcontroller. In addition to controlling the gain scheduling and multiplexing, it provides an on chip Analog-to-Digital converter to read the sensor values, and communicates with the host computer.

## 2.2 Sensor Characterization

The sensors can be characterized simply numerically, that is, by measuring their response as a function of distance and angle, and processing this data purely numerically. However, in order to simplify on-line processing, an analytical model of each sensor was obtained by fitting a calibration set of data to a functional relation.

The sensors' output  $h$ , was modelled as a function of the sensor-object distance,  $d$ , the sensor-object angle,  $\theta$ , and the object's surface properties (roughness, color, etc.) collectively labelled as the reflectance gain,  $\lambda$ . The relation between sensor output and  $d$  was an inverse power, usually two [4, 9, 12]. The surface was assumed to be Lambertian and thus the sensor output was considered to vary with the cosine of sensor-object angle,  $\theta$  [7, 9]. Finally the reflectance gain,  $\lambda$ , was assumed to be a simple gain [4, 12], resulting in the sensor model

$$h_i(d_i, \theta_i, \lambda) = \frac{\lambda \beta_{1,i}}{(d_i + \beta_{4,i})^{\beta_{2,i}}} \cos(\beta_{3,i} \theta_i). \quad (1)$$

The index  $i$  indicates the  $i^{\text{th}}$  sensor in the PSN. The parameters,  $\beta_{1-4,i}$  were obtained by fitting a calibration data set to this model using recursive least squares. Due to the manual manufacture of the sensors, each sensor's parameters were slightly different.

The calibration set was obtained by measuring the sensor output as a white bond paper covered cylinder 65.5 mm in diameter was moved in front of the sensor. Considering that the center of the sensor's face was the origin of a cartesian coordinate system with the sensor's line of sight collinear with the  $q_3$ -axis, the cylinder's centre was swept

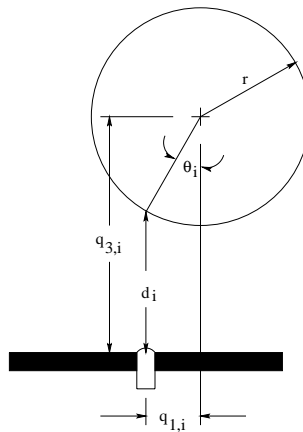


Figure 1: *Sensor-local variable assignments.*

between  $-45 < q_3 < +45$  mm and  $0 < q_1 < 250$  mm in 1 mm steps. Each cartesian coordinate pair was then transformed to a distance and angle pair via

$$\theta_i = \text{asin}\left(\frac{q_{1,i}}{r}\right), \quad d_i = q_{3,i} - r \cos(\theta_i). \quad (2)$$

Since the arcsine is not defined when  $\|q_{1,i}\| > r$ , all data for which this inequality holds were eliminated from the calibration data set. Refer to Fig. 1 for a graphical representation of the relationship between the cartesian coordinates and the sensor geometric parameters.

Since the calibration was performed using white paper, we set the reflectance gain  $\lambda$  (arbitrarily) to unity for this surface. The fit between the experimental data and the model was evaluated by examining the error surface between the two sets, shown for one sensor in Fig. 2. The error surface has been projected onto the error-angle and the error-distance planes to emphasize the systematic errors in the fit. There are significant errors at angles larger than  $\pm 65$  degrees and at distances less than 10 mm. Although these errors are cause for concern, the model was considered satisfactory as the errors in most of the calibrated region were small. Furthermore, the successful object state estimation despite these errors points to the strong robustness of our approach.

## 3 Data Fusion

Measurements from the PSN sensors are non-linear, noisy, and configuration dependent. In addition, autonomous grasping requires real-time identification of the parameters and state. For these reasons, an extended Kalman filter (EKF) with linearization of the observation equation was selected to perform data fusion for the PSN.

A PSN sensing an object is shown in Fig. 3. The object is modelled as free-flying, treating any accelerations as disturbances. Its kinematic states are the position and velocity of its center. The object's reflectance gain,  $\lambda$ , is appended to the state

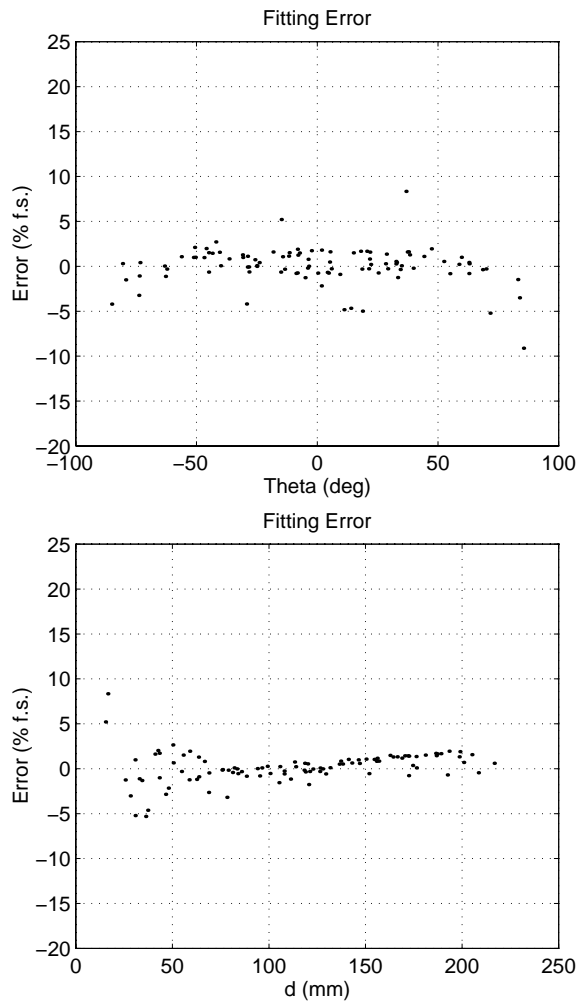


Figure 2: Projection of error plot between the analytical sensor model and the experimental data onto the error- $\theta$  plane (top) and the error- $d$  plane (bottom).

vector so that it may be estimated simultaneously. The discrete state equation is therefore

$$x_{k+1} = \Phi x_k + w_k \quad (3)$$

where

$$x_k = [q_1, \dot{q}_1, q_2, \dot{q}_2, \lambda]^T$$

$$\Phi = \begin{pmatrix} \xi & 0_{2 \times 2} & 0_{2 \times 1} \\ 0_{2 \times 2} & \xi & 0_{2 \times 1} \\ 0_{1 \times 2} & 0_{1 \times 2} & 1 \end{pmatrix}$$

$$\xi = \begin{pmatrix} 1 & \tau \\ 0 & 1 \end{pmatrix}$$

and  $\tau$  is the sampling period. The system is observed with the measurement equation

$$y_k = h(x_k) + v_k, \quad (4)$$

where  $h$  is the sensor model described in Sec. 2.2.

The noise processes are assumed be zero mean gaussian, with

$$E[v_k v_l] = R\delta_{kl}, \quad E[w_k w_l] = Q\delta_{kl}$$

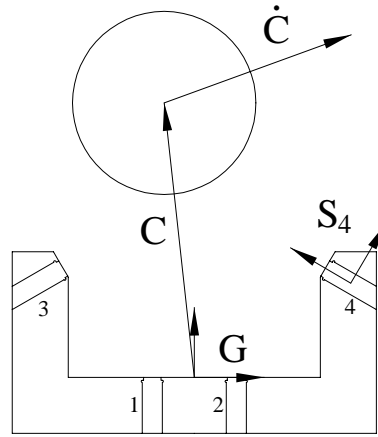


Figure 3: PSN sensing an object. Position,  $C$ , and velocity,  $\dot{C}$ , are estimated with respect to gripper-local coordinates,  $G$ , but transformed to each of the four sensor-local coordinates, ( $S_4$  shown), when evaluating the measurement equation  $h(x)$ .

representing the constant sensor noise covariance and state error covariance matrices, respectively.

The estimation procedure is performed by an Extended Kalman Filter:

*Prediction*

$$x_{k+1|k} = \Phi x_k \quad (5)$$

$$P_{k+1|k} = \Phi P_k \Phi^T + Q$$

*Update*

$$x_{k+1|k+1} = x_{k+1|k} + K[y_{meas,k+1} - h(x_{k+1|k})]$$

$$P_{k+1|k+1} = S P_{k+1|k} S^T + K R K^T$$

where

$$S = [I - K H_{k+1}],$$

and the Kalman gain is

$$K = P_{k|k-1} H_k^T [H_k P_{k|k-1} H_k^T + R]^{-1},$$

with

$$H_k = \left[ \frac{\partial h(x)}{\partial x} \right]_{x=x_{k+1|k}}$$

and  $P$  is the state covariance matrix. Known sensor displacements, for example due to robot movement, would be added to the RHS of (3) and (5).

The state variables must be transformed from end-effector-fixed coordinates to sensor-local coordinates using the transformation matrix

$${}^S i T_G = \begin{bmatrix} \cos \alpha_i & -\sin \alpha_i & S i_x \\ \sin \alpha_i & \cos \alpha_i & S i_y \\ 0 & 0 & 1 \end{bmatrix}$$

where  $\alpha_i$  is the angle between the x-axis of the end-effector and sensor coordinate systems, and  $S i_x, S i_y$  are the components of the distance between the origins of the two coordinate systems.

The transformed state vector is then used to calculate the sensor model’s variables,  $d$  and  $\theta$ .

The sensor noise covariance matrix  $R$  is a diagonal matrix, since we assume no sensor cross coupling. Its entries are a measure of confidence in the sensor inputs and model, and are affected by sensor noise, modelling errors, and inaccuracies in sensor placement. In our experimental setup the unit matrix  $R = I$  was a reasonable setting across all experimental runs.

The value of each element in the model noise covariance matrix  $Q$  is a measure of the filter’s confidence in its model for that state. As with  $R$ , only the elements on the diagonal were non-zero. The tradeoff in tuning  $Q$  is between estimate accuracy at steady state and robustness to disturbances, including eliminating state errors at initialization. For all the experiments we found that  $Q = [1, 2, 0.1, 0.5, 0.001]$  provided the best performance. Both covariance matrices were left unchanged for all the experiments described below.

## 4 Experiments

The experiments were conducted on a planar robotic testbed. The robot is a PPR (prismatic-prismatic-revolute) manipulator with a dextrous workspace [2] of 0.6 m x 0.3 m. Control and data acquisition was done via a two node INMOS transputer network.

The system’s ability to locate an object was demonstrated experimentally. For each experiment the PSN was mounted in a fixture whose position relative to the robot’s workspace was known. The object was fixed to the robot so that its trajectories could be controlled as well as sensed. Data from the PSN as well as from the robot mounted sensors were collected and saved. The results from three experiments are presented and discussed below.

### 4.1 Position Estimation

In this first experiment, the task was for the stationary sensor to estimate the location (and reflectance gain) of the stationary object. As can be seen from Fig. 4, the filter’s estimates for the planar position converged to within 0.5 mm of the correct value, despite large initial errors. The velocities, not shown for brevity, converged to zero. Finally, the reflectance gain was estimated accurately as well.

### 4.2 Reflectance Gain Estimation

In this experiment a band of black paper was wrapped around the cylindrical object. Half-way through the experiment this band was slipped up

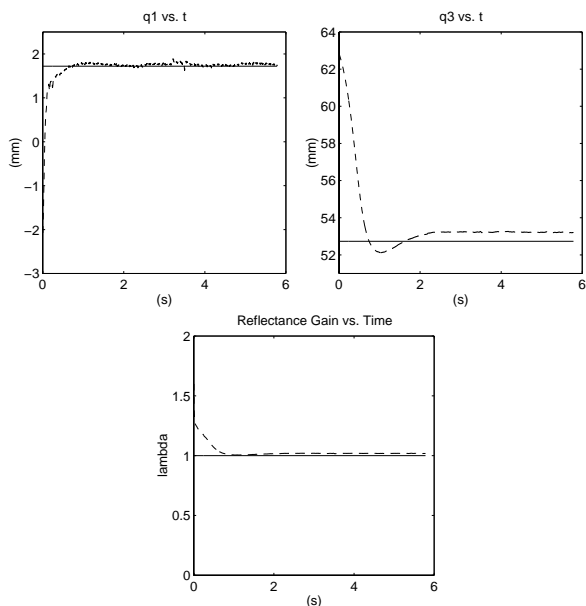


Figure 4: *Position (top) and reflectance gain (bottom) estimation for a stationary object. The actual values are shown as solid lines.*

and off the object by hand to reveal the white surface. The object remained stationary.

This experiment tested the system in two ways. Initially it provided the system’s response when presented with an object whose surface properties differed from those of the object with which the sensors were calibrated. Secondly, it tested its response to a step change in reflectance gain. Black was chosen as a worst case scenario in terms of reflectance gain.

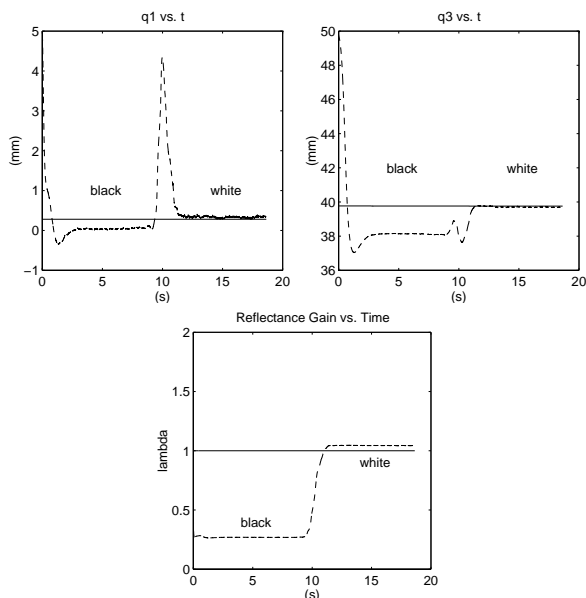


Figure 5: *State estimation of a stationary object which undergoes a step change in reflectance gain when the object color changes from black to white.*

The results are shown in Fig. 5. For the first 10

seconds the object was black. As can be seen, the estimates of all the states converge quickly from their initial values. Thus the system can be used on objects with different surface properties. This is a significant improvement over those systems which use numerical sensor characterization since a new calibration would have to be performed for each color the system would encounter.

When the black band was removed we note from the bottom panel that the change in reflectance gain was detected and converged quickly. In the other panels it can be seen that the position and velocity estimates, after some transients, return to steady state. There is a difference between the position estimate before and after the color change. The position estimate is better for an object with a high reflectance gain due to a corresponding increase in the signal to noise ratio. It should be noted that in spite of the poorer performance with the black object, the estimate is still reasonable with submillimeter error in  $q_1$  and a two millimeter error in  $q_3$ . This is a worst case scenario which would be avoided in practice.

### 4.3 Full State Estimation

This experiment demonstrates the system's ability to estimate the position of an object which violates the linear motion assumption of the Kalman filter (3). The robot was programmed to move the object towards the PSN fixture along a sinusoidal trajectory with an amplitude of 8 mm and a frequency was 0.5 Hz. As can be seen in Fig. 6, the object trajectory as well as the object's reflectance gain was estimated faithfully once the initial errors were overcome. Again the object velocity estimations are omitted for brevity.

## 5 Conclusions

This paper described a system composed of a Proximity Sensor Network (PSN) with four intensity-based electro-optical proximity sensors and an Extended Kalman Filter. This system permits the simultaneous estimation of an object's reflectance properties, allows for angle dependent sensor models, all while tracking it's trajectory. Experiments show robust position estimation of the moving object, despite noisy sensor data, inaccuracies in the sensor model, unmodelled object dynamics and changing reflectance gain. The resulting system will be used for sensor-based control of dynamic grasping and manipulation in robotics and automation.

Current research addresses several issues. First, a supervisory level is needed to initialize and monitor the state estimates. Second, other object geometries are investigated. Third, we are developing a limited form of object recognition by monitoring the trace of the state covariance matrix.

Finally, we are trying to reduce the number of sensor necessary, while preserving the current system's robustness to modelling errors and initialization errors.

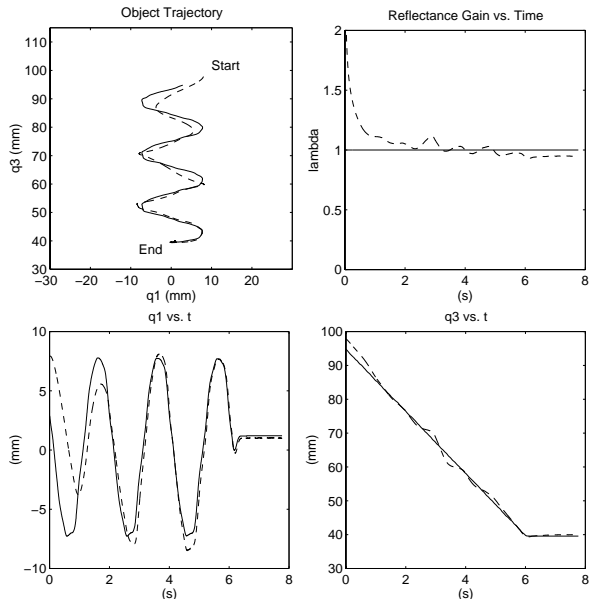


Figure 6: *State estimation of a moving object which is undergoing continuous changes in reflectance gain. Actual and estimated trajectories are given in the top panel. Note that in spite of unmodelled object dynamics as well as changes in reflectance gain the object's position is still estimated with a high degree of accuracy.*

## Acknowledgements

Support for this research was provided in part by the Institute for Robotics and Intelligent Systems (IRIS), a federally-funded Network of Centers of Excellence. Support for GP was provided by Québec's Fonds pour la Formation de Chercheurs et l'Aide à la Recherche (FCAR). The authors would like to thank J. Damianakis for his help in setting up the experimental testbed used for this research.

## References

- [1] M. Buehler, D. E. Koditschek, and P. J. Kindlmann. Planning and Control of Robotic Juggling and Catching Tasks. *Int. J. Robotics Research*, 13(2):101–118, 1994.
- [2] J.J. Craig. *Introduction to Robotics Mechanics and Control*. Addison Wesley, Reading, MA, 1986.
- [3] H.A. Ernst. *MH-1, a computer-operated mechanical hand*. PhD thesis, M.I.T., Dec 1961.

- [4] B. Espiau and J.Y. Catros. Use of optical reflectance sensors in robotics applications. *IEEE Trans. Systems, Man, and Cybernetics*, 10(12):903–912, Dec 1980.
- [5] S. C. Jacobsen, F. M. Smith, E. K. Iversen, and D. K. Backman. High performance, high dexterity, force reflexive teleoperator. In *Proc. 38th Conf. Remote Systems Technology*, pages 180–185, Albuquerque, NM, Feb 1990.
- [6] A.R. Johnston. Proximity sensing technology for manipulator end effectors. *Mechanism and Machine Theory*, 12:95–109, 1977.
- [7] S.M. Juds. *Photoelectric Sensors and Controls*. Marcel Dekker, Inc., NY, 1988.
- [8] L. Korba, S. Elgazzar, and T. Welch. Active infrared sensors for mobile robots. *IEEE Trans. Instrumentation and Measurement*, 43(2):283–7, Apr 1994.
- [9] M. D. Levine. *Vision in Man and Machine*. McGraw Hill, Montreal, 1985.
- [10] Y.F. Li. Extended kalman filtering for robotic proximity sensing. *Proc. 30th Conf. Decision and Control*, 30(5):1041–1042, 1991.
- [11] Y.F. Li. Robot end-effector orientation control using proximity sensors. *Robotics and Computer-Integrated Manufacturing*, 10(5):323–331, 1993.
- [12] Y.F. Li. Characteristics and signal processing of a proximity sensor. *Robotica*, 12:335–41, 1994.
- [13] Y.F. Li. A proximity sensor and its application in real-time control. *Robotics and Autonomous Systems*, 13:25–37, 1994.
- [14] R. Masuda. Multifunctional optical proximity sensor using phase modulation. *J. Robotic Systems*, 3(2):137–147, 1986.
- [15] O. Partaatmadja, B. Benhabib, and A. Goldenberg. Analysis and design of a robotic distance sensor. *J. Robotic Systems*, 10(4):427–445, 1993.
- [16] G. Petryk and M. Buehler. Dynamic object localization via a proximity sensor network. In *IEEE/SICE/RSJ Int. Conf. Multisensor Fusion and Integration for Intelligent Systems*, pages 337–341, Washington, DC, Dec 1996.
- [17] A.A. Rizzi and D.E. Koditschek. Further progress in robot juggling: The spatial two-juggle. In *Proc. IEEE Int. Conf. Robotics and Automation*, Atlanta, GA, May 1993.
- [18] G. Skofte and G. Hirzinger. Computing position and orientation of a freeflying polyhedron from 3d data. *Proc. IEEE Int. Conf. Robotics and Automation*, pages 150–155, Apr 1991.
- [19] C. Wampler. Multiprocessor control of a telemanipulator with optical proximity sensors. *Int. J. Robotics Research*, 3(1):40–50, 1984.